Redox Biology 36 (2020) 101602

Contents lists available at ScienceDirect

Redox Biology

journal homepage: www.elsevier.com/locate/redox

The role of the myeloperoxidase-derived oxidant hypothiocyanous acid (HOSCN) in the induction of mitochondrial dysfunction in macrophages

Dominic T. Love[a,b,1], Chaorui Guo[c], Evelina I. Nikelshparg[d], Nadezda A. Brazhe[d], Olga Sosnovtseva[c], Clare L. Hawkins[a,b,c,*]

[a] The Heart Research Institute, 7 Eliza Street, Newtown, NSW, 2042, Australia
[b] Sydney Medical School, University of Sydney, NSW, 2006, Australia
[c] Department of Biomedical Sciences, University of Copenhagen, Panum, Blegdamsvej 3B, Copenhagen N, DK-2200, Denmark
[d] Department of Biophysics, Biological Faculty, Moscow State University, Leninskie Gory 1/12, Moscow, 119234, Russia

ARTICLE INFO

Keywords:
Myeloperoxidase
Thiocyanate
Hypothiocyanous acid
Mitochondria
Inflammation
Atherosclerosis
Raman spectroscopy

ABSTRACT

A host of chronic inflammatory diseases are accelerated by the formation of the powerful oxidant hypochlorous acid (HOCl) by myeloperoxidase (MPO). In the presence of thiocyanate (SCN^-), the production of HOCl by MPO is decreased in favour of the formation of a milder oxidant, hypothiocyanous acid (HOSCN). The role of HOSCN in disease has not been fully elucidated, though there is increasing interest in using SCN^- therapeutically in different disease settings. Unlike HOCl, HOSCN can be detoxified by thioredoxin reductase, and reacts selectively with thiols to result in reversible modifications, which could potentially reduce the extent of MPO-induced damage during chronic inflammation. In this study, we show that exposure of macrophages, a key inflammatory cell type, to HOSCN results in the reversible modification of multiple mitochondrial proteins, leading to increased mitochondrial membrane permeability, decreased oxidative phosphorylation and reduced formation of ATP. The increased permeability and reduction in ATP could be reversed by pre-treatment of the macrophages with cyclosporine A, implicating a role for the mitochondrial permeability transition pore. HOSCN also drives cells to utilise fatty acids as an energetic substrate after the inhibition of oxidative phosphorylation. Raman imaging studies highlighted the ability of HOSCN to perturb the electron transport chain of mitochondria and redistribute these organelles within the cell. Taken together, these data provide new insight into the pathways by which HOSCN can induce cytotoxicity and cellular damage, which may have relevance for the development of inflammatory disease, and therapeutic strategies to reduce HOCl-induced damage by supplementation with SCN^-.

1. Introduction

Mammalian heme peroxidases, such as myeloperoxidase (MPO), eosinophil peroxidase (EPO) and lactoperoxidase (LPO), play a crucial role in the detoxification of invading pathogens as part of the innate immune response [1]. These heme peroxidases catalyse the reaction of H_2O_2 with halide and pseudo-halide ions to form alternative chemical oxidants, including hypochlorous acid (HOCl), hypobromous acid (HOBr) and hypothiocyanous acid (HOSCN), which are critical in bacterial cell killing and the prevention of bacterial growth [2,3]. However, in addition to their role in immune defence, a large body of evidence implicates these oxidants, particularly HOCl and HOBr, in the induction of oxidative tissue damage and the progression of chronic inflammatory disease [1,4,5]. As such, there is significant interest in gaining a greater understanding of the biological reactivity of peroxidase-derived oxidants as a means to develop novel therapeutic approaches to prevent damaging reactions *in vivo*, and the subsequent propagation of inflammatory disease.

The role of HOSCN in disease, in contrast to HOCl and HOBr, has not been as fully elucidated. It has been suggested that HOSCN formation could be detrimental, on the basis of alterations in redox signalling and the induction of cellular dysfunction on exposure of different cell models to this oxidant (reviewed [6–8]). However, there is also increasing evidence to support a beneficial role of supplementation with thiocyanate (SCN^-) to reduce inflammatory disease by favouring the formation of HOSCN compared to HOCl by MPO [9–11]. The

* Corresponding author. Department of Biomedical Sciences, University of Copenhagen, Panum, Blegdamsvej 3B, Copenhagen N, DK-2200, Denmark.
E-mail address: clare.hawkins@sund.ku.dk (C.L. Hawkins).
[1] Present address: Uppsala University, Department of Immunology, Genetics and Pathology, Rudbeck Laboratory, Dag Hammarskjöldsv. 20, 751 85, Uppsala, Sweden.

https://doi.org/10.1016/j.redox.2020.101602
Received 13 April 2020; Received in revised form 20 May 2020; Accepted 3 June 2020
Available online 10 June 2020
2213-2317/ © 2020 The Authors. Published by Elsevier B.V. This is an open access article under the CC BY-NC-ND license (http://creativecommons.org/licenses/BY-NC-ND/4.0/).

Abbreviations

ANT	adenine nucleotide translocator
BSA	bovine serum albumin
CCCP	carbonyl cyanide *m*-chlorophenyl hydrazone
CPT	carnitine palmitoyltransferase
CsA	cyclosporine A
DMEM	Dulbecco's modified Eagle's medium
EDTA	ethylenediaminetetraacetic acid
EPO	eosinophil peroxidase
ETC	electron transport chain
Eto	etomoxir
FAO	fatty acid oxidation
FBS	fetal bovine serum
FCCP	carbonyl cyanide-*4*-(trifluoromethoxy)phenylhydrazone
GAPDH	glyceraldehyde 3-phosphate dehydrogenase
HBSS	Hanks balanced salt solution
HOBr	hypobromous acid
HOCl	hypochlorous acid
HCAEC	human coronary artery endothelial cells
HOSCN	hypothiocyanous acid
LPO	lactoperoxidase
MPO	myeloperoxidase
MPTP	mitochondrial permeability transition
NFκB	nuclear factor κB
OCR	oxygen consumption rate
Palm-BSA	palmitate-BSA
PMSF	phenylmethylsulfonyl fluoride
PVDF	polyvinylidene fluoride
RCR	respiratory control ratio
SDT	sodium dithionite
SERCA	sarco/endoplasmic reticulum Ca^{2+}-ATPase
SCN^-	thiocyanate
TCA	tricarboxylic acid
TrxR	thioredoxin reductase
VLCAD	very long chain acyl-coenzyme A dehydrogenases

pathways responsible for these protective effects are not fully characterised, but are postulated to be associated with the greater selectivity of HOSCN compared to HOCl, the formation of reversible oxidation products, and the greater ability of HOSCN to be detoxified by intracellular antioxidant enzymes such as thioredoxin reductase (TrxR) (reviewed [3,6,9]).

In light of the potential therapeutic applications of HOSCN, and because even under normal physiological halide and pseudo-halide concentrations (140 mM Cl^-, 20–100 μM Br^-, < 1 μM I^-, 50–100 μM SCN^-), almost half of the H_2O_2 employed by MPO is used to produce HOSCN [12,13], there is interest in understanding the cellular reactivity of HOSCN. HOSCN reacts selectively with thiols (R–SH), which results in the formation of sulfenyl thiocyanate (RS-SCN) species, that can be hydrolysed to sulfenic acids or react further to form disulfides [14,15]. There is also evidence for the formation of sulfinic and sulfonic acids on exposure of isolated proteins to a molar excess of HOSCN [15]. Exposure of cells to HOSCN results in the formation of reversible thiol oxidation products, including sulfenic acids, on a range of intracellular proteins, which is associated with loss in enzymatic activity [16].

HOSCN targets the glycolytic enzymes in the cells, including glyceraldehyde 3-phosphate dehydrogenase (GAPDH) [15,16], protein tyrosine phosphatases (PTPs) [17,18], caspases [19], lysosomal cathepsins B and L [20] and the sarco/endoplasmic reticulum Ca^{2+}-ATPase (SERCA) [21], which has a range of detrimental cellular effects (reviewed [8]). HOSCN can also target redox-sensitive transcription factors, including nuclear factor κB (NFκB), which promotes the release of various pro-inflammatory mediators and decreases cellular survival [22–24]. Bolus addition of HOSCN to different cell types results in cell death by both necrotic and apoptotic pathways [8], which is associated with protein thiol oxidation [25] and loss in mitochondrial membrane permeability [26].

Although HOSCN alters mitochondrial membrane permeability, the mechanisms responsible for this have not been elucidated. Similarly, the effects of HOSCN on cellular energy production by oxidative phosphorylation or the β-oxidation of fatty acids have not been characterised, although this oxidant has been shown to decrease glycolysis and ATP production in macrophages [16]. This, together with the abundance of protein thiols within mitochondria and their role in the regulation and activity of the tricarboxylic acid (TCA) cycle and mitochondrial oxidative phosphorylation [27,28], led us to examine the ability of HOSCN to target mitochondrial thiol-containing proteins, particularly those of the electron transport chain (ETC) [29]. We also determined the effects of this oxidant on oxidative phosphorylation and fatty acid oxidation in real time using a Seahorse analyser, as both are crucial energetic processes that occur within the mitochondria. We also utilised Raman approaches for the first time to provide additional insight into understanding the how HOSCN alters the ETC of mitochondria and their distribution within the cell.

2. Materials and methods

2.1. Materials and Reagents

All aqueous reagents were prepared using nanopure water, filtered through a four stage Milli-Q system. All reagents were from Sigma Aldrich (St Louis, MO, USA) unless otherwise noted. HOSCN was prepared enzymatically with lactoperoxidase (LPO; from bovine milk) using LPO/H_2O_2/SCN^- as described previously [25,30], with the concentration determined by quantifying the consumption of 5-thio-2- nitrobenzoic acid (TNB) at 412 nm [31] using a molar absorption coefficient of 14,150 M^{-1} cm^{-1} [32].

2.2. Cell culture

Murine macrophage-like J774A.1 cells (American Type Culture Collection; No. 915051511) were cultured under sterile conditions in Dulbecco's modified Eagle's medium (DMEM) supplemented with 10% (v/v) fetal bovine serum (ThermoFisher Scientific, Waltham, MA, USA) and 2 mM L-glutamine at 37 °C in a 5% CO_2 incubator. Unless otherwise noted, cells were seeded in 12-well culture plates at a density of 1 × 10^6 cells/well and allowed to adhere overnight. Except where stated otherwise, cells were washed in Hanks balanced salt solution (HBSS) prior to treatment with HOSCN, which was diluted into HBSS immediately before addition to the cells.

2.3. Protein sulfenic acid formation

J774A.1 cells (3 × 10^6 cells) were treated with DCP-Bio1 (Kerafast, Boston, MA, USA; 500 μM) in DMEM for 1 h at 37 °C and 5% CO_2. The cells were washed three times with HBSS and then exposed to HOSCN (0–200 μM) in HBSS for 1 h at 22 °C. After treatment, cells were washed three times with HBSS before separation of the cytosol and mitochondrial fractions with a mitochondrial isolation kit (ThermoFisher Scientific) using the supplier's instructions. After isolation, the mitochondria were lysed using a mitochondrial lysis buffer (75 μL; 0.5% Triton X-100; 30 mM Tris, pH 7.4; 200 mM KCl; 5 mM ethylenediaminetetraacetic acid [EDTA]; 0.5 mM phenylmethylsulfonyl fluoride [PMSF]; 1x protease inhibitors) with vigorous vortexing for 1 min. Protein concentration was determined using a DC Lowry protein assay (Bio-Rad, Hercules, CA, USA). SDS-PAGE was used to separate proteins

and was carried out using either 10- or 12-well pre-cast mini-format 4–12% acrylamide Bis-Tris gels (Life Technologies, Carlsbad, CA, USA). Samples were loaded into wells and separated at 80 V until the dye front reached the gel interface. Following electrophoresis, proteins were transferred to polyvinylidene fluoride (PVDF) membranes. The membrane was blocked in 3% (w/v) bovine serum albumin (BSA) in PBS containing Tween 20 (PBST, 0.1% v/v Tween 20) overnight at 4 °C. The membrane was then washed with PBST (3 × 10 min) and incubated with 1:10000 horseradish peroxidase (HRP)-streptavidin in 3% (w/v) BSA-PBST for 1 h at 22 °C. Finally, the membrane was washed with PBST and immunodetection was performed using ECL Plus chemiluminescence reagents (PerkinElmer, Waltham, MA, USA), and detected by a ChemiDoc XRS (Bio-Rad).

2.4. Functional mitochondrial respiration assays

Seahorse XF-24 cell culture plates were coated with 3.5 μg/cm^2 of Cell-Tak cell and tissue adhesive (Becton-Dickinson, North Ryde, NSW, Australia) prior to seeding J774A.1 cells (7.5 × 10^4 cells). Cells were equilibrated for 1 h at 37 °C in XF base media (0.8 mM $MgSO_4$, 1.8 mM $CaCl_2$, 143 mM NaCl, 5.4 mM KCl, 0.91 mM NaH_2PO_4, 3 mg mL^{-1} phenol red, with 2 mM L-glutamine added immediately prior to use). After equilibration, cells were exposed to HOSCN (0–150 μM) in XF base media (containing 2 mM L-glutamine, 40 mM sodium pyruvate and 10 mM glucose) for 1 h at 22 °C, prior to measuring oxygen consumption rate (OCR). The media was then replaced with fresh XF base media and the XF Cell Mitochondrial Stress Test was performed using the following injection media: Port A: oligomycin (1.5 μM), Port B: FCCP (0.5 μM) and Port C: rotenone (0.5 μM) and antimycin A (0.5 μM) using a Seahorse XF-24 Extracellular Analyser (Agilent, Santa Clara CA, USA). After the completion of the assay, the cells were washed and lysed in 25 μL RIPA buffer (150 mM NaCl, 1.0% IGEPAL CA-630, 0.5% sodium deoxycholate, 0.1% SDS, and 50 mM Tris, pH 8.0) and a DC Lowry protein assay was performed to normalise the data to protein concentration. These data were then used to calculate: basal respiration (basal OCR before injections – non-mitochondrial respiration), ATP-linked respiration (basal OCR – OCR following oligomycin injection), proton leak (OCR following oligomycin injection – non-mitochondrial respiration), ETC accelerator response or maximal respiration (maximum OCR after FCCP injection – non-mitochondrial respiration), spare (reserve) respiratory capacity as a % (maximal respiration/basal respiration x 100) and coupling efficiency (ATP-linked respiration/basal respiration x 100).

2.5. Functional fatty acid β-oxidation assay

J774A.1 cells were incubated in substrate-limited medium (0.5 mM glucose, 1 mM L-glutamine, 0.5 mM carnitine and 1% FBS) at 37 °C in a 5% CO_2 incubator for 24 h prior to washing and seeding in Cell-Tak precoated XF-24 cell culture plates as described above. Cells were equilibrated using XF base media supplemented with 2.5 mM glucose, 0.5 mM carnitine, 5 mM HEPES and respective substrates for β-oxidation (palmitate-BSA or unconjugated BSA; 50 μM) adjusted to pH 7.4 for 1 h at 37 °C. The media was removed and the cells were then exposed to HOSCN (100 μM) or potassium phosphate buffer (pH 6.6) in XF base media (containing 2.5 mM glucose, 0.5 mM carnitine, 5 mM HEPES) for 1 h at 22 °C. Where appropriate, etomoxir (Eto; 37.5 μL of 40 μM) was added 15 min before the start of the assay. The media was once again removed and replaced with fresh XF base media and the OCR was measured using the Seahorse analyser immediately after the addition of XF palmitate-BSA or unconjugated BSA substrate (150 μM) to the wells. The XF Cell FAO Stress Test was performed using the following injection media: Port A: oligomycin (1.5 μM), Port B: FCCP (1.0 μM) and Port C: rotenone (0.5 μM) and antimycin A (0.5 μM). After the completion of the assay, the cells were washed and lysed in 25 μL RIPA buffer and a DC Lowry protein assay was performed to normalise the data to protein concentration.

2.6. Mitochondrial depolarisation

Mitochondrial membrane potential was assessed using the MitoProbe JC-1 assay kit for flow cytometry (Molecular Probes, Eugene, OR, USA). The J774A.1 cells (1 × 10^6 cells) were treated with HOSCN (0–200 μM) in HBSS for 1 h at 22 °C, before detaching the cells by gentle scraping and resuspending in HBSS and incubation with JC-1 (2 μM) for 15 min at 37 °C in a 5% CO_2 incubator. Flow cytometry analysis was performed using a Cytomics FC500 flow cytometer (Beckman Coulter).

2.7. Intracellular Ca2+ determination

Measurement of intracellular Ca^{2+} was performed using Fluo-4AM (Life Technologies). Cells (1 × 10^6) were treated with HOSCN (0–200 μM) for 1 h in Ca^{2+} supplemented HBSS or Ca^{2+} free HBSS, followed by incubation with Fluo-4AM (5 μM) for 15 min, before washing and lifting into suspension by gentle scraping. Flow cytometry analysis was performed on a FACSVerse flow cytometer (BD Biosciences).

2.8. Raman spectroscopy

J774A.1 cells (5 × 10^5 cells) were seeded on 35 mm Petri dishes with a 14 mm glass bottom in DMEM (2 mL of medium per dish). Before recording the Raman spectra, the cells were washed and incubated in HBSS solution in the absence and presence of HOSCN (200 μM) for 1 h at 22 °C. An inVia confocal Raman microspectrometer (Renishaw, UK) equipped with a 532 nm laser was used to record the spectra of the cells with objective x63, NA 0.9. The laser power per registration spot was no more than 0.5 mW and the spectrum accumulation time was 10 s. Raman spectra were recorded from at least 6 cells per dish from the cytoplasm region around the nucleus of a living cell following treatment. A small amount of sodium dithionite (SDT) powder was added to both HOSCN-treated and control cells 5 min before repeating the measurements of Raman spectra to reduce all mitochondrial cytochromes.

2.9. Raman imaging and Raman mapping

Raman imaging was performed in the map mode of the InVia Raman microspectrometer with the distance between registration points equaled to 1 μm. Raman spectra at each point were recorded with the laser power 0.5 mW with an accumulation time of 2 s. Raman images were recorded from the same cell before and 1 h following exposure to HOSCN, and again 5 min following addition to SDT.

2.10. Analysis of Raman spectra and Raman images

Resonance Raman spectra and images were processed with open source software Pyraman http://bitbucket.org/alexeybrazhe/pyraman after performing baseline subtraction. The parameters for baseline subtraction were chosen after the processing of approximately 40 spectra from different cells. After the baseline subtraction, the intensities of the peaks of interest were defined and ratios of Raman intensities were calculated. RMS (root-mean-square) value was determined for the following intervals: 500-540 cm^{-1}, 740-750 cm^{-1} and 1630-1680 cm^{-1} and Raman maps were plotted of ratios: $RMS_{740-750}/RMS_{500-540}$, $RMS_{1630-1680}/RMS_{500-540}$ and $RMS_{740-750}/RMS_{1630-1660}$.

2.11. Statistical analyses

Statistical analyses were performed using GraphPad Prism (versions 6.0–8.0; GraphPad Software, San Diego, USA) using one-way or two-

way ANOVA with Tukey's multiple comparison post-hoc test with $p < 0.05$ taken as significant. Details of specific tests are outlined in the Figure Legends.

3. Results

3.1. Reaction of HOSCN thiol-containing proteins in the cytosol and mitochondria of J774A.1 cells

Exposure of J774A.1 cells to HOSCN has been shown previously to result in formation of reversible thiol oxidation products, including sulfenic acids, on a range of intracellular proteins [15,16]. Therefore, in this study, we used the sulfenic acid-sensitive probe, DCP-Bio1, in conjunction with immunoblotting, to examine whether thiol-containing proteins localised in the mitochondria were targets of HOSCN. J774A.1 cells were pre-treated with DCP-Bio1 (500 μM) before the addition of HOSCN (0–200 μM), and isolation of the mitochondria. Following separation of the resulting cellular fractions, a significant increase in the staining intensity and band density was observed on analysis of both the cytosolic and mitochondrial fractions, following exposure of the cells to HOSCN (Fig. 1). The staining density was greater with increasing concentrations of HOSCN (Fig. S1), consistent with the dose-dependent formation of protein sulfenic acids on a range of cytosolic and mitochondrial proteins.

After imaging, the membranes were stripped and re-probed for β-actin and COX4 as a loading control and to confirm the purity of the cytosolic and mitochondrial fractions. The cytosolic fractions contained a similar amount of protein in each case, as assessed by comparable β-actin staining, and lacked the mitochondrial protein COX4 (Fig. S1). In contrast, the mitochondrial fractions contained COX4, which was present at similar amounts in each fraction, consistent with equivalent protein loading. The mitochondrial fractions also showed a very low level of staining for β-actin (Fig. S1). This may reflect some residual contamination of the mitochondrial fractions with cytosolic proteins. However, the pattern of DCP-Bio1 staining observed on exposure of the cells to HOSCN is different in the cytosolic and mitochondrial fractions, consistent with isolation of the mitochondria from the cytosol (Fig. 1).

3.2. HOSCN attenuates oxidative phosphorylation in J774A.1 cells

Having shown that HOSCN can react with a range of thiol-containing proteins in the mitochondria, functional assays were then performed using a Seahorse XF 24 analyser, to assess whether the exposure of HOSCN to J774A.1 macrophages resulted in altered oxidative phosphorylation. Initial studies were performed to assess the effect of HOSCN on basal respiration in the J774A.1 cells (7.5×10^4) exposed to HOSCN (0–150 μM) for 1 h. This treatment resulted in a dose-dependent decrease in basal respiration as reflected by a marked decrease in OCR with increasing concentrations of HOSCN (Fig. 2A). These studies were extended by performing a mitochondrial stress test, to measure changes in OCR and the ability of J774A.1 cells to respond to the disruption of mitochondrial processes following the sequential injection of a series of inhibitors and uncoupling agents (Fig. 2B).

Exposure of the J774A.1 cells to HOSCN (0–150 μM) for 1 h resulted in a significant decrease in the ATP-linked respiration following injection of oligomycin, which inhibits ATP production by blocking the F0 subunit of ATP synthase (Fig. 3B), in addition to the marked decrease in basal respiration (Fig. 3A). A significant decrease in the ETC accelerator response or maximal respiration was also observed following injection of FCCP (Fig. 3C), indicating that HOSCN plays a direct role in the disorder of the proton gradient. This is partially reflected in the proton leak measurements, which decreases with HOSCN concentrations < 100 μM and is increased at higher oxidant concentrations (Fig. 3D). There was no apparent change in the spare (reserve) respiratory capacity (Fig. 3E), explained by the ratiometic decrease in both the maximum respiration and basal respiration, whereas a decrease in the coupling efficiency was observed (Fig. 3F). Exposure of the cells to HOSCN had no significant effect on the non-mitochondrial respiration, which was determined after injection of rotenone and antimycin A to inhibit the ETC (Fig. 2B). Taken together, these data show that exposure of cells to HOSCN decreases basal respiration, and reduces the efficiency of ATP formation by the mitochondria, related to uncontrolled proton leakage in a HOSCN-dependent manner.

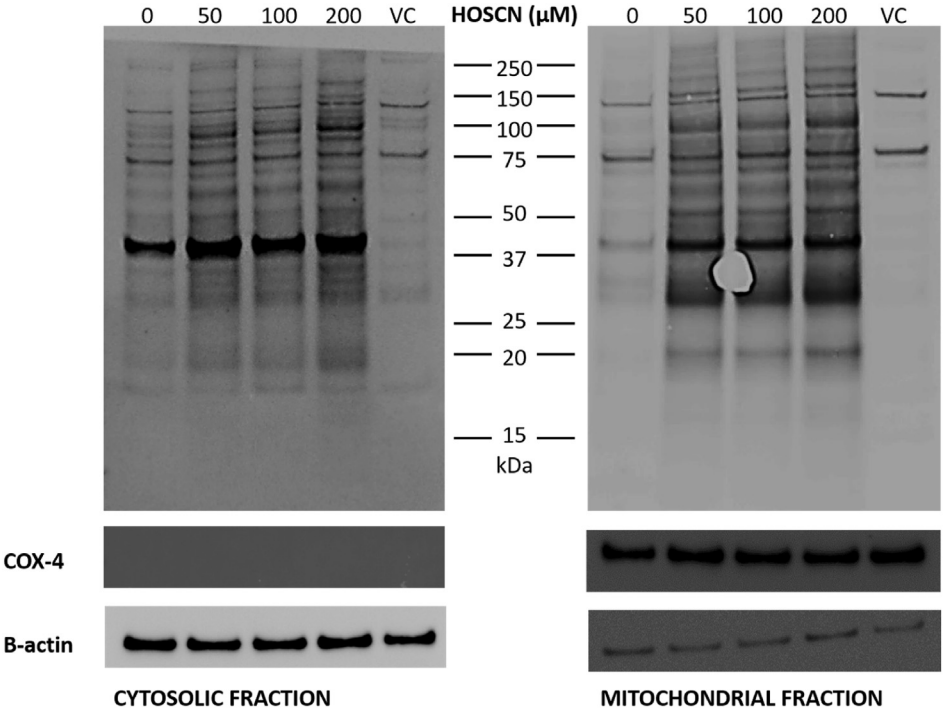

Fig. 1. HOSCN induces sulfenic acid formation in the cytosol and mitochondria of J774A.1 cells. J774A.1 cells (3×10^6 cells) were pre-treated the sulfenic acid probe, DCP-Bio1 (500 μM) or a DMSO vehicle control (VC) for 1 h at 37 °C prior to the addition of HOSCN (0–200 μM) and further incubation for 1 h at 22 °C. Panel A shows the cytosolic fraction and panel B shows the mitochondrial fraction following probing for DCP-Bio1, with COX-4 used as a mitochondrial protein loading control, and β-actin used for cytosolic protein detection. Images are representative of 3 independent experiments.

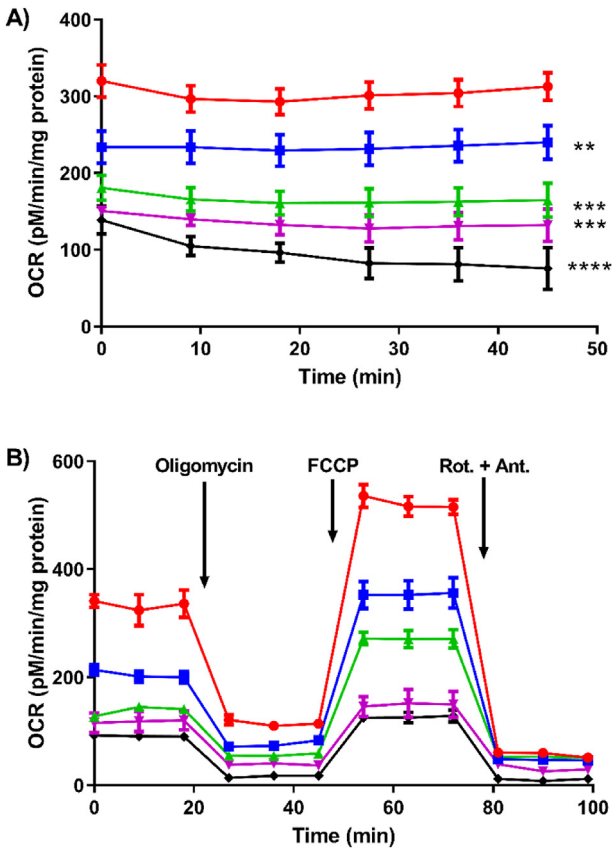

Fig. 2. Effect of HOSCN on the oxygen consumption profile of J774A.1 cells. Treatment of J774A.1 cells (7.5×10^4 cells) with 0 (red circle), 50 (blue square), 75 (green triangle), 100 (pink triangle), 150 (black diamond) μM HOSCN for 1 h at 22 °C in the presence of XF base media, with OCR measured using a Seahorse XF 24 Extracellular analyser. (A) shows the effect of HOSCN on basal oxygen consumption after a 15 min equilibration phase; (B) shows the profile from the mitochondrial stress test after sequential injections oligomycin (1.5 μM), FCCP (0.5 μM), and rotenone and antimycin A (Rot. + Ant.; 0.5 μM). Data represent the mean ± S.E.M. of 3 independent experiments. **, ***, and **** show a significant ($p < 0.01$, 0.001, and 0.0001) decrease on comparison of the HOSCN treatments to the non-treated control by repeated measures two way ANOVA with a Tukey's post hoc test. (For interpretation of the references to colour in this figure legend, the reader is referred to the Web version of this article.)

3.3. HOSCN increases mitochondrial membrane permeability in the J774A.1 cells

To further characterise the HOSCN-induced changes to mitochondrial respiration and examine proton leakage across the mitochondrial membrane, the permeability of the mitochondrial membrane was examined. Cells were exposed to HOSCN (0–200 μM) for 1 h before being washed to remove any residual oxidant and labelled with JC-1, which exhibits potential-dependent accumulation in mitochondria. Flow cytometry analysis revealed a dose-dependent loss of red fluorescent JC-1 aggregates in the mitochondria and a corresponding increase in green fluorescent JC-1 within the cytosol under these treatment conditions (Fig. S2). The decrease in the ratio of red:green JC-1 fluorescence observed on exposure of the cells to HOSCN (Fig. 4A) is consistent with depolarisation of the mitochondrial membrane and a corresponding increase in mitochondrial membrane permeability (Fig. 4A). The decrease in red:green JC-1 fluorescence was significant on comparison of the non-treated control cells with cells treated with HOSCN concentrations > 50 μM, where marked perturbations in oxidative phosphorylation were also apparent. The loss in membrane permeability seen with the highest concentration of HOSCN (200 μM) was comparable to that observed on treating the cells with the mitochondrial uncoupling agent carbonyl cyanide *m*-chlorophenyl hydrazone (CCCP; 2 μM, 15 min at 37 °C) (Fig. 4A).

The role of the mitochondrial permeability transition pore (MPTP) in the HOSCN-induced depolarisation of the mitochondrial membrane was examined in experiments where the cells were pre-treated with cyclosporine A (CsA) to inhibit the opening of the MPTP. The J774A.1 cells were pre-treated with CsA (1 μM, for 1 h at 22 °C) prior to the addition of HOSCN (0–200 μM) for 1 h at 22 °C and assessment of the mitochondrial membrane permeability with JC-1. Pre-treatment of the cells with CsA decreased the extent of loss of mitochondrial membrane permeability observed on exposure of the cells to HOSCN (Fig. 4B). The effect of HOSCN on the MPTP and ATP production was examined further by comparing the levels of intracellular ATP on exposure of the cells to HOSCN in the presence and absence of pre-treatment with CsA (1 μM). Treatment of the J774A.1 cells with HOSCN (50–200 μM) resulted in a significant, dose-dependent decrease in intracellular ATP (Fig. 4C), which supports the change observed in coupling efficiency (Fig. 3F). The extent of loss in ATP was decreased on pre-treatment of the cells with CsA (Fig. 4C). Taken together, these data are consistent with HOSCN playing a role in the opening of the MPTP, which decreases oxidative phosphorylation and ATP production.

The MPTP is highly sensitive to Ca^{2+} [33], therefore additional experiments were performed to assess alterations in intracellular Ca^{2+} using flow cytometry with Fluo-4 AM. However, there were no apparent changes in the concentration of intracellular Ca^{2+} following treatment of the J774A.1 cells with HOSCN (50–200 μM) for 1 h (Fig. S3). This suggests that the observed altered mitochondrial membrane permeability may not be triggered by HOSCN-induced changes in intracellular Ca^{2+}.

3.4. J774A.1 cells are able to maintain fatty acid oxidation after HOSCN treatment

Given the effect of HOSCN on oxidative phosphorylation in J774A.1 cells and our previous data showing comparable decreases in glycolysis [16], we next examined the effects of HOSCN treatment on fatty acid oxidation (FAO) using the Seahorse XF 24 analyser to measure OCR using palmitate conjugated to BSA (Palm-BSA) as a substrate. J774A.1 cells (7.5×10^4) were exposed to HOSCN (100 μM) for 1 h before the sequential addition of oligomycin, FCCP and rotenone/antimycin A in the presence of BSA alone, Palm-BSA or Palm-BSA after pre-treatment of the cells with the carnitine palmitoyltransferase (CPT) 1 inhibitor, etomoxir (Eto; 40 μM) to prevent the transport of fatty acyl moieties into the mitochondria. It should be noted that the concentration of glucose used in these experiments (2.5 mM) was lower than that employed in the mitochondrial respiration experiments (10 mM). In the control, non-treated cells, there was a small, but non-significant increase in OCR under basal conditions in the cells containing Palm-BSA compared to BSA alone or Palm-BSA with Eto pre-treatment (Fig. 5A). There was also a small, but non-significant increase in basal OCR in the HOSCN-treated cells containing Palm-BSA on comparison to BSA alone or Palm-BSA with Eto pre-treatment (Fig. 5B). Under basal conditions, the change in OCR observed in the presence of Palm-BSA compared to BSA was similar with both the control and HOSCN-treated cells, indicating that HOSCN has no positive or inhibitory effect on basal FAO (Fig. 5C).

Upon injection with FCCP, a small but non-significant decrease in OCR was observed in the non-treated cells under all conditions (BSA, Palm-BSA, Palm-BSA + Eto). This can be compared to the data from the mitochondrial stress test, where an increase in the OCR and ETC accelerator response is seen in the non-treated cells (Fig. 3C). This suggests that glucose catabolism and oxidative phosphorylation is preferable to utilisation of fatty acids by the J774A.1 cells (Fig. 5A). However, this decrease in OCR after FCCP injection does not occur in HOSCN-treated J774A.1 cells in the presence of Palm-BSA, in contrast to the

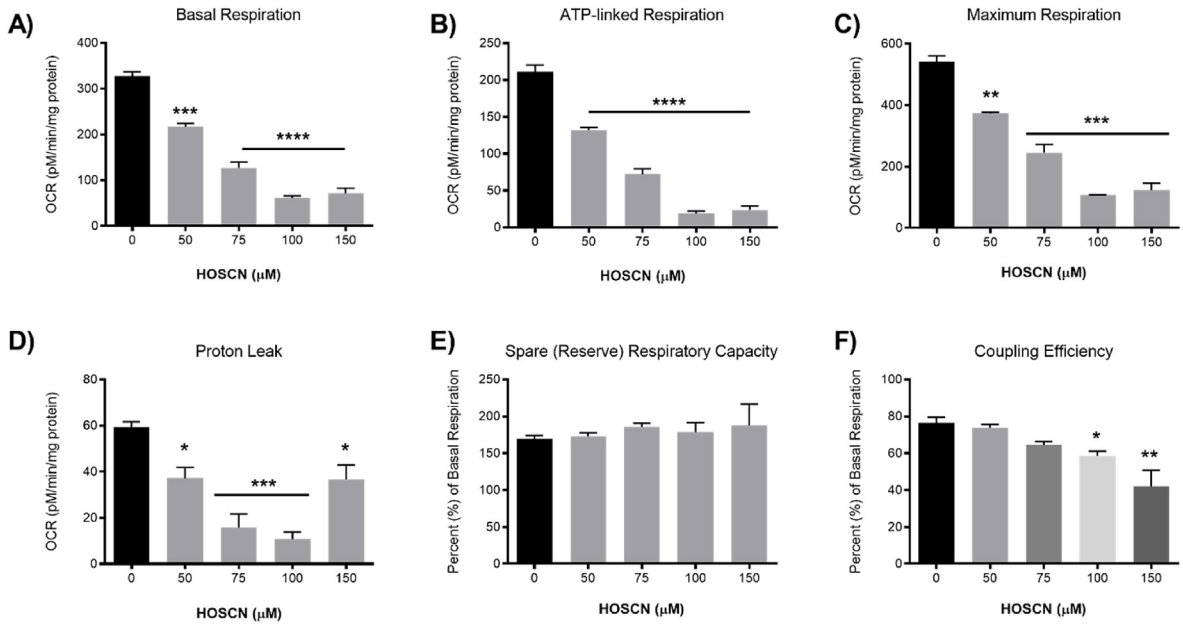

Fig. 3. HOSCN treatment decreases mitochondrial respiration. J774A.1 cells (7.5 × 10^4 cells) were treated with HOSCN (0–150 μM) for 1 h at 22 °C in the presence of XF base media, before performing the mitochondrial stress test and recording OCR with sequential injections of oligomycin (1.5 μM), FCCP (0.5 μM), and rotenone and antimycin A (0.5 μM) using a Seahorse XF 24 Extracellular Analyser. Graphs show (A) OCR under basal conditions, (B) ATP-linked respiration (after oligomycin), (C) maximum respiration (after FCCP), (D) proton leak, (E) spare/reserve respiratory capacity as % (maximum respiration/basal respiration x 100) and (F) coupling efficiency (ATP-linked respiration/basal respiration x 100). Data represent the mean ± S.E.M. of 3 independent experiments. *, **, ***, and **** show a significant ($p < 0.05$, 0.01, 0.001, and 0.0001) difference between HOSCN treatment and the non-treated control cells by repeated measures one-way ANOVA with a Tukey's post hoc test.

decrease of OCR and the ETC accelerator response observed in mitochondrial stress test (Fig. 3C). These data suggest that HOSCN-treated J774A.1 cells can maintain the capacity to utilise substrates for FAO and energy production (Fig. 5D).

3.5. Redox state of mitochondrial cytochromes following HOSCN treatment

The effect of HOSCN on the redox state of mitochondrial cytochromes was examined using Raman spectroscopy with 532 nm excitation, to visualize peaks associated with the hemes in mitochondrial *c* and *b*-type cytochromes, together with those from lipids and proteins. Representative Raman spectra from both control and HOSCN-treated J774A.1 cells, together with the region of spectrum acquisition are shown in Fig. 6. Peaks with maxima positions at 747, 1124, 1308, 1338 and 1583 cm^{-1} are assigned to the vibrations of bonds of hemes in reduced *c* and *b*-type cytochromes (Table S1) [34–39]. As Raman scattering of oxidized cytochromes is non-intensive and cannot be detected in living cells [34–36,38,39], we applied the reducing reagent SDT to reduce any oxidized ETC components. Addition of SDT to the cells resulted in an increase in the intensities of the peaks at 747 and 1124 cm^{-1} (Fig. 6A and B, red spectra), consistent with the reduction of *c*-type and *b*-type mitochondrial cytochromes, respectively, allowing the total amount of mitochondrial *c* and *b*-type cytochromes present in the mitochondria to be assessed. Peaks with maxima positions at 1003 and 1660 cm^{-1} correspond to the vibrations associated with the aromatic ring of Phe residues and the C–N peptide bond of proteins, respectively, whereas the peak at 1445 cm^{-1} is assigned to the C–C bond vibrations characteristic of mainly lipids, but also some proteins (Table S1) [37,40,41].

Exposure of the J774A.1 cells to HOSCN resulted in a significant decrease in the relative amounts of reduced *c* and *b*-type cytochromes when compared to the protein content, on calculation of the ratios of the intensities of the cytochrome peaks at 747 cm^{-1} (mainly cytochrome type *c* and *c*1) and 1124 cm^{-1} (mainly *b*-type cytochromes) to the protein peak at 1003 cm^{-1} (I_{747}/I_{1003} and I_{1124}/I_{1003} shown in Fig. 7A and B). A decrease in the relative amount of all *c* and *b*-type cytochromes was also apparent in cells after HOSCN treatment, on calculating the same peak intensity ratios but following addition of SDT to reduce the cytochromes (Fig. 7C and D). In contrast, there was no difference in the relative amount of either the reduced or total cytochrome *c* molecules compared to the cytochromes *b* molecules (I_{747}/I_{1124} and I_{747}/I_{1124} with SDT; Fig. S4). Similarly, there was also no significant difference between the relative amount of lipids compared to proteins in the cells after HOSCN treatment (I_{1445}/I_{1660}, Fig. S4).

Raman imaging experiments were also performed on several cells before and after exposure to HOSCN, and following the addition of SDT, to enable distribution maps to be plotted of the *c*-type cytochromes (747 cm^{-1}), as a marker of mitochondria, compared to proteins (1660 cm^{-1}) within each cell. The Raman map showing the relative amount of reduced *c*-type cytochromes in the non-treated cells on normalization to the spectral background noise is shown in Fig. 8D. This map shows the non-homogenous distribution of the reduced *c*-type cytochromes, consistent with a non-even distribution of the mitochondria within the macrophages. Similar data are observed on normalization of the reduced *c*-type cytochromes to protein (Fig. 8J).

The application of HOSCN to the cells resulted in a decrease in Raman intensities calculated for the region 740–750 cm^{-1} on normalization to both the background (Fig. 8E) or protein (Fig. 8K), consistent with oxidation of the *c*-type cytochromes. Addition of SDT significantly increased the Raman intensities calculated for the region 740–750 cm^{-1} compared to the intensities seen before and after HOSCN treatment (Fig. 8F, L). Interestingly, there is no overlap in the regions with the highest Raman intensities reflecting the *c*-type cytochromes after addition of SDT, with the brightest regions in the cell before SDT application (Fig. 8). This could reflect rearrangement of the mitochondria inside cells after exposure to HOSCN or/and SDT treatment.

4. Discussion

It is well established that HOSCN targets thiol-containing proteins

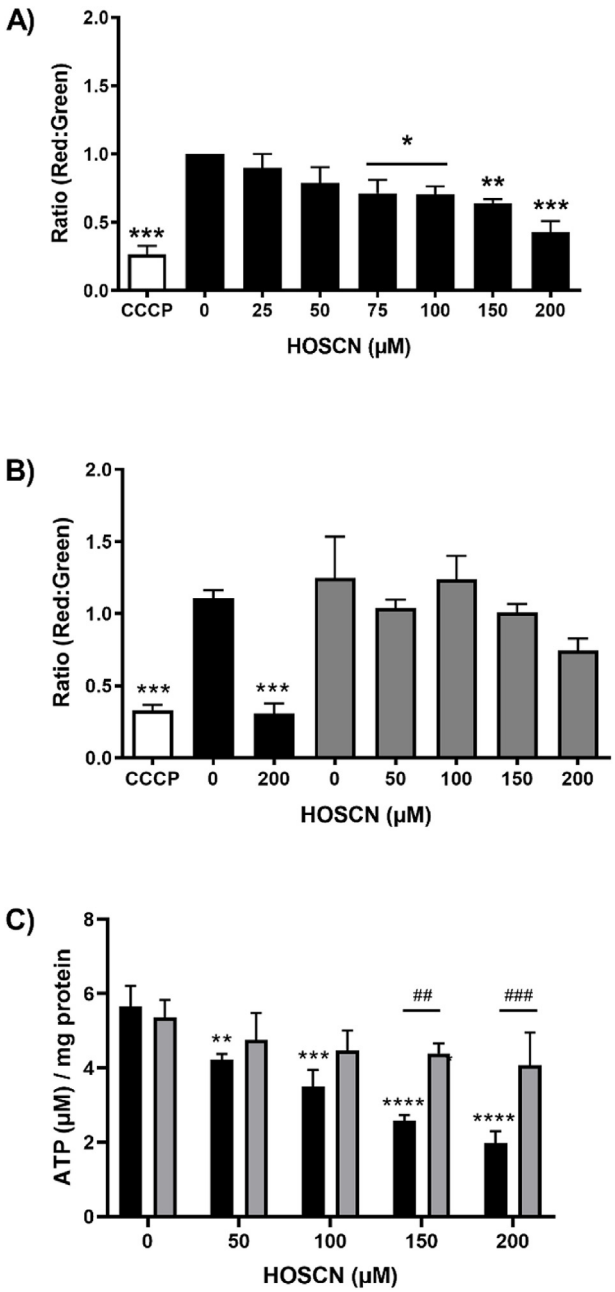

Fig. 4. HOSCN increases mitochondrial membrane depolarisation and decreases ATP production. J774A.1 cells (1×10^6 cells) were treated with HOSCN (0–200 μM, black bars) for 1 h at 22 °C. In (A) and (B) treatment with CCCP (5 μM, white bars) for 10 min at 37 °C was included as a positive control, before labelling with JC-1 (2 μM) and flow cytometry to assess alterations in the ratio of red fluorescent mitochondrial JC-1 aggregates to green fluorescent cytosolic JC-1. In (B) experiments were also performed with cells pre-treated with cyclosporine A (CsA; 1 μM, grey bars) for 1 h prior to addition of HOSCN. Graph (C) shows the effect of HOSCN on cellular ATP levels in J774A.1 cells (1×10^6 cells) with (grey bars) and without (black bars) CsA (1 μM) pre-treatment. Data represent the mean ± S.E.M. of 3 independent experiments. *, **, *** and **** show a significant ($p < 0.05$, 0.01, 0.001 and 0.0001) difference between HOSCN treatment and the non-treated control cells by repeated measures one-way ANOVA with a Dunnett's post hoc test. ## and ### show a significant ($p < 0.01$ and 0.001) difference on comparing with and without CsA pre-treatment by two way ANOVA with Sidak's post-hoc test.

within cells, which can influence both the function and viability of different cell types (reviewed [7,8]). HOSCN induces reversible oxidation of cellular thiols, and promotes the formation of different reversible oxidation products, including protein-derived sulfenic acids [15,16]. In this study, we demonstrated that HOSCN targets mitochondrial protein thiols, in addition to cytosolic protein thiols, as evidenced by an increase in the formation of protein sulfenic acids, visualised using the probe DCP-Bio1. In addition to thiol oxidation, treatment of the J774A.1 cells with HOSCN resulted in a decrease in mitochondrial respiration and ATP concentrations, together with an increase in mitochondrial membrane permeability. Pre-treatment of the cells with CsA decreased this increase in mitochondrial membrane permeability and reduced the extent of ATP loss, consistent with HOSCN altering the MPTP. HOSCN also altered mitochondrial FAO and changed the redox state of mitochondrial *c*- and *b*-type cytochromes in J774A.1 cells.

Evidence was obtained for a dose-dependent increase in the formation of sulfenic acids on a mixture of cytosolic and mitochondrial proteins following exposure of the J774A.1 cells to HOSCN, as reflected by the intensity of staining of the DCP-Bio1 probe. The pattern of staining observed is consistent with the reaction of HOSCN with multiple mitochondrial thiol-containing proteins, as well as cytosolic proteins. Whether the altered mitochondrial membrane permeability induced by HOSCN influences the accessibility of the DCP-Bio1 probe to the mitochondria and hence the detection of protein sulfenic acids is not known. However, DCP-Bio1 does not generally localise in mitochondria, including when cells are stressed with t-butyl-hydroperoxide [42]. The extent of formation of protein sulfenic acids seen in the J774A.1 cells exposed to HOSCN agrees well with previous data from this cell type showing loss of the total cellular pool of protein thiols on addition of HOSCN [25] and the formation of reversible oxidation products on cytosolic proteins [16]. In this study, the specific identity of the mitochondrial proteins targeted by HOSCN in J774A.1 cells was not examined given the dynamic nature of the thiol modifications and abundance of some of the mitochondrial proteins. However, evidence was obtained through experiments with CsA, for a role of the MPTP, which influenced HOSCN-induced mitochondrial membrane depolarisation and loss in ATP production.

The marked effect of HOSCN on mitochondrial respiration, permeability and ATP production seen in the J774A.1 cells could reflect the direct oxidation of mitochondrial thiol-containing proteins, particularly those associated with energy production and the transport of electrons. Mitochondrial ETC enzymes contain critical thiols and iron-sulfur clusters, which play an important role in the regulation and activity of the TCA cycle and mitochondrial oxidative phosphorylation [27–29]. Thus, oxidation of critical thiols in mitochondrial complexes I and II by ebselen and related organochalcogen compounds, diphenyl diselenide and diphenyl ditelluride, is known to inhibit activity [43,44]. In addition, studies with isolated mitochondria show that exposure to trichlorotelluro-dypnones decreases the concentration of thiols, which correlates with a decrease in state 3 and state 4 respiration and reduction of the respiratory control ratio (RCR) [45]. RCR can only be measured in isolated mitochondria, but a decrease in the RCR indicates a decrease in substrate oxidation and ATP turnover, and a high proton leak, supporting the results in our cell-based study with HOSCN.

Other studies have shown that the ETC complexes I, II and V, ATP synthase together with aconitase, and several other TCA cycle enzymes are sensitive to glutathionylation, which results in the loss of enzymatic activity, and is therefore a potential pathway to mitochondrial dysfunction (reviewed [46]). Protein glutathionylation in vascular smooth muscle cells following their exposure to diamide, resulted in a marked decrease in OCR, consistent with altered mitochondrial respiration [47]. Whether decreased mitochondrial respiration in the J774A.1 cells is driven by glutathionylation of mitochondrial proteins was not examined, but is a possibility in light of the formation of protein sulfenic acids, which could react further with GSH [48].

Aconitase is known to be a target for HOSCN in a cellular environment, with a loss in aconitase activity and an increase of iron release from the iron-sulfur cluster of cytosolic aconitase observed on

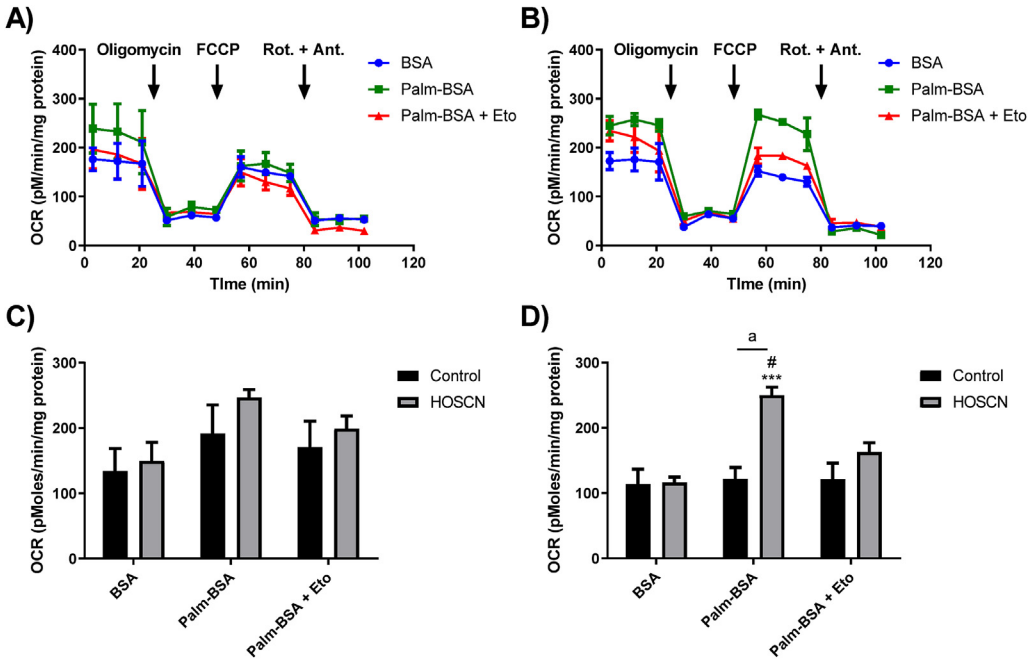

Fig. 5. Effect of HOSCN on fatty acid oxidation in J774A.1 cells. J774A.1 cells (7.5×10^4 cells) were incubated in the absence of (A) or the presence of (B) HOSCN (100 μM) for 1 h at 22 °C prior to measuring the OCR using a Seahorse XF 24 Extracellular analyser after sequential injections of oligomycin (1.5 μM), FCCP (0.5 μM), and rotenone and antimycin A (Rot. + Ant.; 0.5 μM) in the presence of BSA alone (BSA, blue circle), BSA conjugated to palmitate (Palm-BSA, green square) or palmitate-BSA after pre-treatment with 40 μM Etomoxir (Palm-BSA + Eto, red triangle). (C) shows the change in basal OCR before injection of oligomycin and (D) shows the change in OCR after FCCP injection reflecting maximum respiration in the absence (black bars) and presence (grey bars) of HOSCN. Data represent the mean ± S.E.M. of 3 independent experiments. *** shows a significant ($p < 0.001$) difference between BSA and Palm-BSA reflecting oxidation of exogenous palmitate, # shows a significant ($p < 0.05$) difference between Palm-BSA in the absence and presence of Eto by two way ANOVA with a Tukey's post hoc test. "a" shows a significant ($p < 0.001$) difference on comparing the non-treated control to the HOSCN treatment by two way ANOVA with a Sidak's post-hoc test. (For interpretation of the references to colour in this figure legend, the reader is referred to the Web version of this article.)

exposure of human coronary artery endothelial cells (HCAEC) to HOSCN [49]. This inactivation is observed at comparable oxidant: cell ratios to those employed in the current study with J774A.1 cells, supporting aconitase and the TCA cycle as possible targets for HOSCN in J774A.1 cells. In HCAEC, the loss of aconitase activity was also associated with the formation of iron-response protein 1 and altered iron metabolism, but no measurements were made assess the alteration of mitochondrial function under these treatment conditions [49]. However, other studies with HCAEC have provided evidence for mitochondrial dysfunction and increased cell death by apoptosis on exposure to HOSCN [26].

The inhibition of mitochondrial respiration in cells exposed to HOSCN could also occur indirectly via the lack of glycolysis end-product formation. Our previous study demonstrated that the treatment of J774A.1 cells with HOSCN, under comparable conditions to those used here, resulted in the modification of GAPDH and other glycolytic proteins, which resulted in a marked decrease in ECAR consistent with attenuation of glycolysis [16]. This attenuation of glycolysis resulted in the decreased production of lactate, suggesting a comparable decrease in pyruvate and subsequently acetyl-coA, decreasing the mitochondrial production of NADH (via the TCA cycle) and further potentiating the decrease in oxidative phosphorylation and ATP production.

A further potential contributor to reduced mitochondrial respiration is the observed decrease in the mitochondrial membrane potential. Depolarisation of the mitochondria leads to an increase in permeability, which causes a subsequent loss in protons and small molecules such as cytochrome *c* from the inner mitochondrial space into the cytosol. The loss of the mitochondrial membrane potential is significant at > 50 μM HOSCN treatment concentration, where a significant loss in basal respiration, ATP–linked respiration, maximum respiration, coupling efficiency and cellular ATP levels is also apparent. The loss in ATP production could be largely mitigated by pre-treatment of the cells with CsA, which suggests that HOSCN induces MPTP formation, as CsA blocks the peptidylprolyl isomerase activity of cyclophilin D, which is required for the formation of a complex with the adenine nucleotide translocator (ANT) during MPTP formation (reviewed [50]).

The mechanism by which HOSCN induces MPTP formation is not known. Given that there is no significant change in intracellular Ca^{2+}

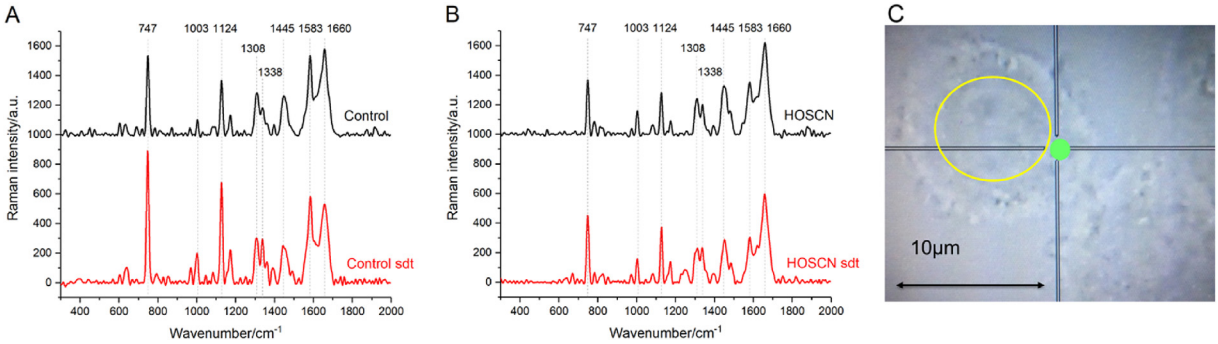

Fig. 6. Effect of HOSCN on the Raman spectra of J774A.1 cells. Representative Raman spectra of (A) control cells and (B) cells treated with HOSCN (200 μM) for 1 h (black lines). The spectra recorded following 5 min incubation of the cells with SDT are shown in red. (C) shows a microphotograph of a control, non-treated cell in the reflected light. The nucleus is shown by the yellow circle. Region of spectrum registration is shown as a green circle. (For interpretation of the references to colour in this figure legend, the reader is referred to the Web version of this article.)

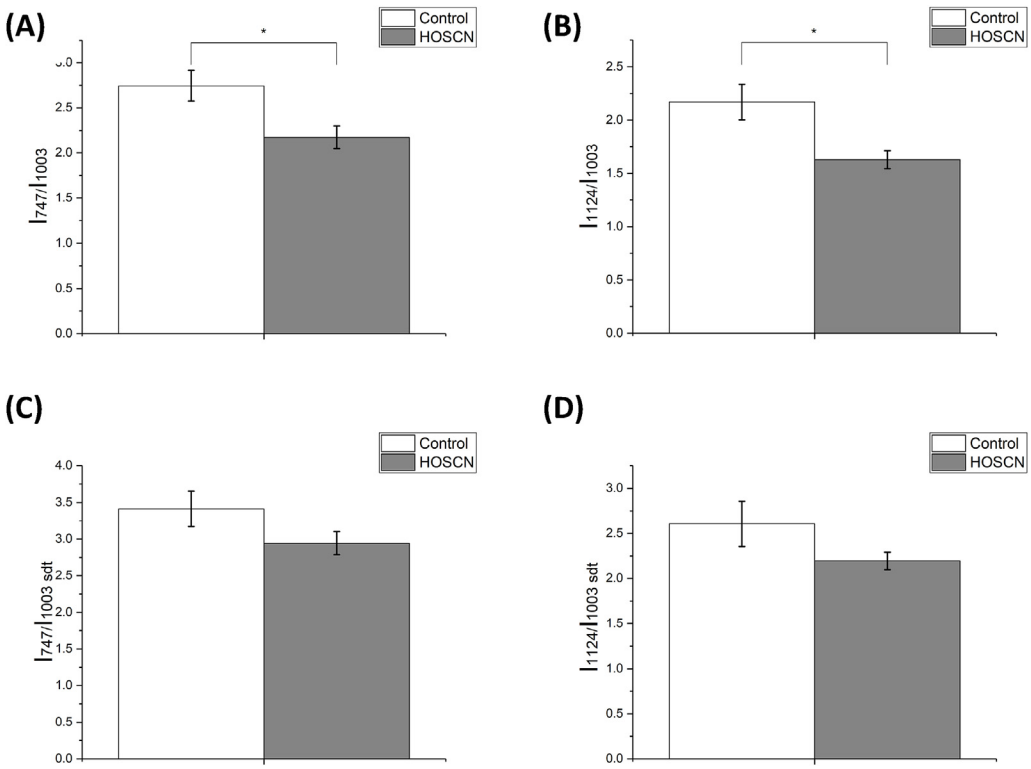

Fig. 7. HOSCN treatment of J774A.1 cells alters the Raman intensity of mitochondrial *c*- and *b*-type cytochromes. Ratios (A) I_{747}/I_{1003} and (B) I_{1124}/I_{1003} in control cells (white bars) and cells after treatment with HOSCN (200 μM) for 1 h (grey bars), which correspond to the amount of reduced *c*-type cytochromes (A) and *b*-type cytochromes (B) normalized to the total protein amount. Ratios (C) and (D) are as (A) and (B) but following addition of SDT. Data represent the mean ± S.E.M. of n = 14 cells. * shows a significant ($p < 0.05$) change with HOSCN treatment using the Mann-Whitney test.

concentrations in the J774A.1 cells exposed to HOSCN under conditions where changes in mitochondrial function are apparent, it is perhaps more likely that the effects observed are related to oxidation of key proteins involved in the assembly of the MPTP [51]. For example, oxidation of Cys residues on ANT and the formation of a cross-link between Cys_{160} and Cys_{257} on the matrix facing loops prevents ADP-mediated inhibition of the MPTP opening, and results in sensitisation of the MPTP to Ca^{2+} [50,52,53]. It is also possible that HOSCN could induce a conformation change in the MPTP to increase the Ca^{2+} binding sites, as reported previously in studies with isolated mitochondria exposed to *t*-butyl-hydroperoxide [33]. Interestingly, exposure of human monocyte-derived macrophages to HOCl, triggered MPTP formation by alteration of Ca^{2+} fluxes and Ca^{2+}-mediated activation of calpain, resulting in depletion of ATP and necrotic cell death [54], which highlights the difference in the cellular reactivity of HOSCN compared to HOCl [8].

The redox state of mitochondrial NAD(P) has also been linked with MPTP opening [50], with both of these factors known to influence the extent of FAO [55]. There was no significant effect of HOSCN (at 100 μM) on the extent of basal FAO as assessed by the OCR on addition of Palm-BSA, or the BSA only controls (Fig. 5C). It was observed that basal OCR in the FAO assay was consistently lower than OCR recorded in the mitochondrial stress test. The cells were exposed to lower glucose concentrations in the FAO experiments (2.5 mM) compared to the mitochondrial stress test (10 mM). Thus, the lack of a difference in basal OCR in the FAO assay could reflect a reduced flux of glycolytic end-products, which influences the effects of HOSCN on the basal respiration in the J774A.1 cells. However, the OCR was elevated in HOSCN-treated cells when Palm-BSA was available as a substrate for oxidation following addition of FCCP to uncouple the mitochondria.

When comparing this result with the results of the mitochondrial stress test, where HOSCN impairs the ETC accelerator response after FCCP injection (Fig. 3C), it suggests that HOSCN treatment necessitates the utilisation of fatty acids as an energetic substrate. Alterations to the inner mitochondrial membrane permeability, oxidation of mitochondrial thiols together with a decrease in the ratio of $NADH/NAD^+$ can increase FAO in studies with isolated mitochondria [55]. The concentration of mitochondrial NADH was not examined in the study, but our previous work showed that the total cellular NADH decreased on exposure of J774A.1 cells to comparable concentrations of HOSCN [16]. In addition, the "c" conformation of ANT, where the nucleotide binding site faces the cytoplasm that is adopted during FAO [55] is stabilised following thiol oxidation (reviewed [56]), which may also be relevant in cells exposed to HOSCN. It is also possible that the formation of other reversible thiol modifications on mitochondrial proteins by HOSCN could influence the extent of FAO. Thus, *S*-nitrosylation of very long chain acyl-coenzyme A dehydrogenases (VLCAD), which catalyses the rate limiting step in the β-oxidation of fatty acids, activates enzymatic activity by promoting a conformational change that alters the K_M of VLCAD [57].

Further evidence to support a role for HOSCN in modulating the mitochondrial redox state was obtained using Raman spectroscopy. It is widely assumed that only reduced cytochromes *c* and *b* contribute to the Raman spectrum of cells with 532 nm laser excitation, as the Raman scattering of oxidized cytochromes is negligible [34–39], and cytochrome *a/a3* in cytochrome oxidase (complex IV) does not absorb light with this energy [34,38,39]. The Raman data allow us to estimate the relative amount of reduced *b* and *c*-type cytochromes in complex III and cytochrome *c* in the intermembrane space of mitochondria following addition of HOSCN to the cells. The cytochrome *b* present in Complex II is not involved in electron transport, and exists in its oxidized form and therefore does not contribute to the Raman spectra of cells [58]. Our data are consistent with a decrease in the relative amount of reduced *c*- and *b*-type cytochromes on exposure of the cells to HOSCN, which is observed under treatment conditions that also favour decreased ATP production and an increase in reversible thiol oxidation.

The Raman imaging experiments showed that the distribution of reduced *c*-type cytochromes, and hence mitochondria, was not homogenous within the cell. This did not appear to influence the ability of the HOSCN to promote the oxidation of the *c*-type cytochromes. However, the imaging data support the partial degradation of mitochondria and their redistribution inside the cell following exposure to HOSCN. This is

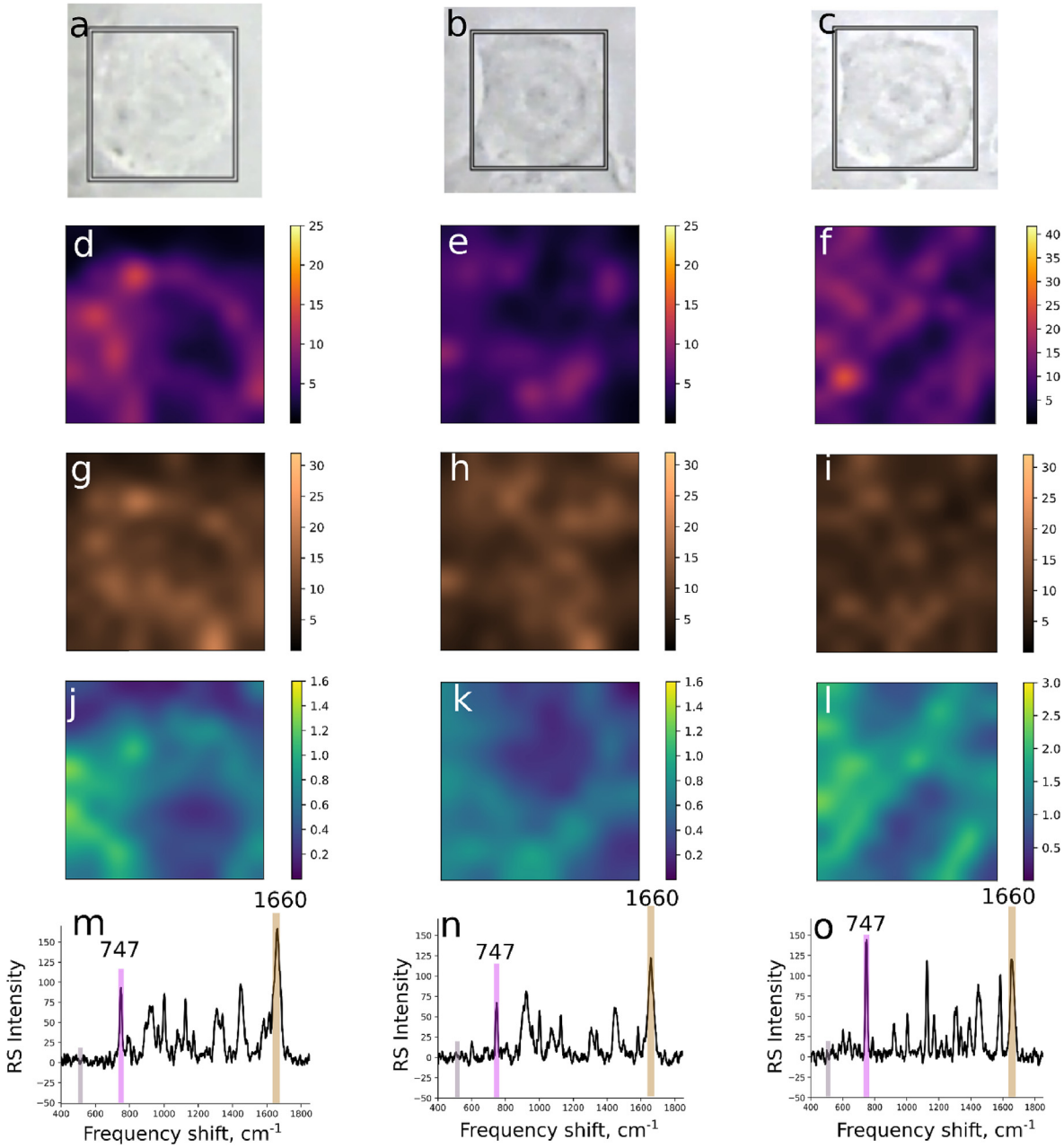

Fig. 8. Raman mapping images of mitochondrial *c*-type cytochromes in J774A.1 cells. First, second and third columns show representative microphotographs (A–C), Raman maps (D–L) and Raman spectra (M–O) plotted for the J774A.1 cell before treatment, after treatment with HOSCN (200 μM) for 1 h, and following treatment with SDT for 5 min, respectively. In (D), (E) and (F) the Raman maps are plotted for RMS values of Raman intensities calculated for the interval 740-750 cm^{-1} (relative amount of *c*-type cytochrome) normalized to the RMS value of the interval 500-540 cm^{-1} (baseline region). In (G), (H) and (I) the Raman maps are plotted for RMS value of Raman intensities calculated for the interval 1630-1680 cm^{-1} (relative amount of all proteins) normalized to the RMS value of Raman intensities of the interval 500-540 cm^{-1} (baseline region). In (J), (K) and (L) the Raman maps are plotted for RMS values of Raman intensities of the interval 740-750 cm^{-1} (relative amount of *c*-type cytochrome) normalized to the RMS value for the interval of 1630–1660 cm^{-1} (relative amount of all proteins). The coloured vertical bars in spectra (M), (N) and (O) highlight the spectral regions used for the RMS calculations.

supported by other cellular models showing the redistribution of mitochondria within cells under conditions of oxidative stress, where altered mitochondrial membrane potential and respiration are also apparent [59].

In this study, the overall cellular consequences of HOSCN-induced mitochondrial dysfunction, and the effect of oxidant treatment on viability were not examined. However, exposure of the J774A.1 cells to HOSCN, at concentrations where a significant loss in basal respiration is apparent (≥50 μM) is associated with non-reversible cell lysis, shown by the leakage of lactate dehydrogenase from the cells [16]. This supports our previous studies showing the ability of HOSCN can induce both necrotic and apoptotic cell death in J774A.1 cells under comparable experimental conditions [25]. Whether the MPTP specifically plays a role in HOSCN-induced necrotic and apoptotic cell death in the J774A.1 cells has not been assessed. Previous studies show that the pathway of cell death induced by exposure to hypohalous acids is highly dependent on the specific treatment conditions as well as the type of cell under study [8]. Indeed, with HOCl, evidence has been presented for a role of the MPTP in the induction of necrotic cell death in macrophages [54], owing to the depletion of ATP, whereas in HepG2 cells, apoptotic cell death via caspase-dependent pathways was seen, following mitochondrial release of cytochrome *c* [60].

In summary, we show that HOSCN induces mitochondrial dysfunction by inducing a decrease in mitochondrial membrane potential, respiration and ATP production, which is associated with formation of the MPTP and alterations to the mitochondrial redox state. These changes are believed to reflect the ability of HOSCN to target multiple mitochondrial proteins containing functionally important thiol groups. The Raman spectroscopy and imaging data highlight a role for HOSCN in inducing the oxidation of mitochondrial *c*- and *b*-type cytochromes, and suggest that exposure of the cells to this oxidant results in the redistribution of the mitochondria within the cells. Overall, these data provide novel mechanistic insight into the pathways by which HOSCN can induce cellular damage and cytotoxicity, which may have relevance for the development of inflammatory pathologies. The data are also important to consider in relation to the implementation of therapeutic strategies to mitigate MPO-induced damage by supplementation with SCN^- to decrease HOCl production.

Declaration of competing interest

None.

Acknowledgements

We would like to thank Prof. Michael Davies for helpful discussions and the Australian Research Council for funding through the Future Fellowship Scheme (FT120100682) for financial support. EIN and NAB acknowledge financial support from Russian Science Foundation (project RSF 17-74-20089).

Appendix A. Supplementary data

Supplementary data to this article can be found online at https://doi.org/10.1016/j.redox.2020.101602.

References

[1] M.J. Davies, C.L. Hawkins, The role of myeloperoxidase in biomolecule modification, chronic inflammation, and disease, Antioxidants Redox Signal. 32 (13) (2020) 957–981.
[2] C.C. Winterbourn, A.J. Kettle, Redox reactions and microbial killing in the neutrophil phagosome, Antioxidants Redox Signal. 18 (6) (2013) 642–660.
[3] B.J. Day, The science of licking your wounds: function of oxidants in the innate immune system, Biochem. Pharmacol. 163 (2019) 451–457.
[4] S.J. Klebanoff, Myeloperoxidase: friend and foe, J. Leukoc. Biol. 77 (2005) 598–625.
[5] J. Wang, A. Slungaard, Role of eosinophil peroxidase in host defence and disease pathology, Arch. Biochem. Biophys. 445 (2) (2006) 256–260.
[6] D.I. Pattison, M.J. Davies, C.L. Hawkins, Reactions and reactivity of myeloperoxidase-derived oxidants: differential biological effects of hypochlorous and hypothiocyanous acids, Free Radic. Res. 46 (8) (2012) 975–995.
[7] T.J. Barrett, C.L. Hawkins, Hypothiocyanous acid: benign or deadly? Chem. Res. Toxicol. 25 (2) (2012) 263–273.
[8] B.S. Rayner, D.T. Love, C.L. Hawkins, Comparative reactivity of myeloperoxidase-derived oxidants with mammalian cells, Free Radic. Biol. Med. 71 (2014) 240–255.
[9] J.D. Chandler, B.J. Day, Biochemical mechanisms and therapeutic potential of pseudohalide thiocyanate in human health, Free Radic. Res. 49 (6) (2015) 695–710.
[10] J.D. Chandler, E. Min, J. Huang, C.S. McElroy, N. Dickerhof, T. Mocatta, A.A. Fletcher, C.M. Evans, L. Liang, M. Patel, A.J. Kettle, D.P. Nichols, B.J. Day, Anti-inflammatory and Anti-microbial effects of thiocyanate in a cystic fibrosis mouse model, Am. J. Respir. Cell Mol. Biol. 53 (2) (2015) 193–205.
[11] P.E. Morgan, R.P. Laura, R.A. Maki, W.F. Reynolds, M.J. Davies, Thiocyanate supplementation decreases atherosclerotic plaque in mice expressing human myeloperoxidase, Free Radic. Res. 49 (6) (2015) 743–749.
[12] C.J. van Dalen, M.W. Whitehouse, C.C. Winterbourn, A.J. Kettle, Thiocyanate and chloride as competing substrates for myeloperoxidase, Biochem. J. 327 (2) (1997) 487–492.
[13] P.E. Morgan, D.I. Pattison, J. Talib, F.A. Summers, J.A. Harmer, D.S. Celermajer, C.L. Hawkins, M.J. Davies, High plasma thiocyanate levels in smokers are a key determinant of thiol oxidation induced by myeloperoxidase, Free Radic. Biol. Med. 51 (9) (2011) 1815–1822.
[14] M.T. Ashby, Inorganic chemistry of defensive peroxidases in the human oral cavity, J. Dent. Res. 87 (10) (2008) 900–914.
[15] T.J. Barrett, D.I. Pattison, S.E. Leonard, K.S. Carroll, M.J. Davies, C.L. Hawkins, Inactivation of thiol-dependent enzymes by hypothiocyanous acid: role of sulfenyl thiocyanate and sulfenic acid intermediates, Free Radic. Biol. Med. 52 (6) (2012) 1075–1085.
[16] D.T. Love, T.J. Barrett, M.Y. White, S.J. Cordwell, M.J. Davies, C.L. Hawkins, Cellular targets of the myeloperoxidase-derived oxidant hypothiocyanous acid (HOSCN) and its role in the inhibition of glycolysis in macrophages, Free Radic. Biol. Med. 94 (2016) 88–98.
[17] A.E. Lane, J.T. Tan, C.L. Hawkins, A.K. Heather, M.J. Davies, The myeloperoxidase-derived oxidant HOSCN inhibits protein tyrosine phosphatases and modulates cell signalling via the mitogen-activated protein kinase (MAPK) pathway in macrophages, Biochem. J. 430 (1) (2010) 161–169.
[18] N.L. Cook, C.H. Moeke, L.I. Fantoni, D.I. Pattison, M.J. Davies, The myeloperoxidase-derived oxidant hypothiocyanous acid inhibits protein tyrosine phosphatases via oxidation of key cysteine residues, Free Radic. Biol. Med. 90 (2016) 195–205.
[19] S.M. Bozonet, A.P. Scott-Thomas, P. Nagy, M.C. Vissers, Hypothiocyanous acid is a potent inhibitor of apoptosis and caspase 3 activation in endothelial cells, Free Radic. Biol. Med. 49 (6) (2010) 1054–1063.
[20] F.O. Ismael, T.J. Barrett, D. Sheipouri, B.E. Brown, M.J. Davies, C.L. Hawkins, Role of myeloperoxidase oxidants in the modulation of cellular lysosomal enzyme function: a contributing factor to macrophage dysfunction in atherosclerosis? PloS One 11 (12) (2016) e0168844.
[21] N.L. Cook, H.M. Viola, V.S. Sharov, L.C. Hool, C. Schoneich, M.J. Davies, Myeloperoxidase-derived oxidants inhibit sarco/endoplasmic reticulum Ca(2+)-ATPase activity and perturb Ca(2+) homeostasis in human coronary artery endothelial cells, Free Radic. Biol. Med. 52 (5) (2012) 951–961.
[22] J.G. Wang, S.A. Mahmud, J. Nguyen, A. Slungaard, Thiocyanate-dependent induction of endothelial cell adhesion molecule expression by phagocyte peroxidases: a novel HOSCN-specific oxidant mechanism to amplify inflammation, J. Immunol. 177 (12) (2006) 8714–8722.
[23] J.G. Wang, S.A. Mahmud, J.A. Thompson, J.G. Geng, N.S. Key, A. Slungaard, The principal eosinophil peroxidase product, HOSCN, is a uniquely potent phagocyte oxidant inducer of endothelial cell tissue factor activity: a potential mechanism for thrombosis in eosinophilic inflammatory states, Blood 107 (2) (2006) 558–565.
[24] G.J. Pan, B.S. Rayner, Y. Zhang, D.M. van Reyk, C.L. Hawkins, A pivotal role for NF-kappaB in the macrophage inflammatory response to the myeloperoxidase oxidant hypothiocyanous acid, Arch. Biochem. Biophys. 642 (2018) 23–30.
[25] M.M. Lloyd, D.M. Van Reyk, M.J. Davies, C.L. Hawkins, HOSCN is a more potent inducer of apoptosis and protein thiol depletion in murine macrophage cells than HOCl or HOBr, Biochem. J. 414 (2) (2008) 271–280.
[26] M.M. Lloyd, M.A. Grima, B.S. Rayner, K.A. Hadfield, M.J. Davies, C.L. Hawkins, Comparative reactivity of the myeloperoxidase-derived oxidants hypochlorous acid and hypothiocyanous acid with human coronary artery endothelial cells, Free Radic. Biol. Med. 65 (2013) 1352–1362.
[27] T. Yagi, Y. Hatefi, Thiols in oxidative phosphorylation: inhibition and energy-potentiated uncoupling by monothiol and dithiol modifiers, Biochemistry 23 (11) (1984) 2449–2455.
[28] T. Yagi, Y. Hatefi, Thiols in oxidative phosphorylation: thiols in the F0 of ATP synthase essential for ATPase activity, Arch. Biochem. Biophys. 254 (1) (1987) 102–109.
[29] S. Drose, U. Brandt, I. Wittig, Mitochondrial respiratory chain complexes as sources and targets of thiol-based redox-regulation, Biochim. Biophys. Acta 1844 (8) (2014) 1344–1354.
[30] C.L. Hawkins, D.I. Pattison, N.R. Stanley, M.J. Davies, Tryptophan residues are targets in hypothiocyanous acid-mediated protein oxidation, Biochem. J. 416 (3) (2008) 441–452.
[31] C.L. Hawkins, P.E. Morgan, M.J. Davies, Quantification of protein modification by oxidants, Free Radic. Biol. Med. 46 (8) (2009) 965–988.
[32] P. Eyer, F. Worek, D. Kiderlen, G. Sinko, A. Stuglin, V. Simeon-Rudolf, E. Reiner, Molar absorption coefficients for the reduced Ellman reagent: reassessment, Anal. Biochem. 312 (2) (2003) 224–227.
[33] N.G. Golovach, V.T. Cheshchevik, E.A. Lapshina, T.V. Ilyich, I.B. Zavodnik, Calcium-induced mitochondrial permeability transitions: parameters of Ca(2+) ion interactions with mitochondria and effects of oxidative agents, J. Membr. Biol. 250 (2) (2017) 225–236.
[34] M. Kakita, V. Kaliaperumal, H.O. Hamaguchi, Resonance Raman quantification of the redox state of cytochromes b and c in-vivo and in-vitro, J. Biophot. 5 (1) (2012) 20–24.
[35] N.A. Brazhe, M. Treiman, A.R. Brazhe, N.L. Find, G.V. Maksimov, O.V. Sosnovtseva, Mapping of redox state of mitochondrial cytochromes in live cardiomyocytes using Raman microspectroscopy, PloS One 7 (9) (2012) e41990.
[36] N.A. Brazhe, M. Treiman, B. Faricelli, J.H. Vestergaard, O. Sosnovtseva, In situ Raman study of redox state changes of mitochondrial cytochromes in a perfused rat heart, PloS One 8 (8) (2013) e70488.
[37] L. Harkness, S.M. Novikov, J. Beermann, S.I. Bozhevolnyi, M. Kassem, Identification of abnormal stem cells using Raman spectroscopy, Stem Cell. Dev. 21 (12) (2012) 2152–2159.
[38] M. Okada, N.I. Smith, A.F. Palonpon, H. Endo, S. Kawata, M. Sodeoka, K. Fujita, Label-free Raman observation of cytochrome c dynamics during apoptosis, Proc. Natl. Acad. Sci. U.S.A. 109 (1) (2012) 28–32.
[39] D.A. Perry, J.W. Salvin, P. Romfh, P. Chen, K. Krishnamurthy, L.M. Thomson, B.D. Polizzotti, F.X. McGowan, D. Vakhshoori, J.N. Kheir, Responsive monitoring of mitochondrial redox states in heart muscle predicts impending cardiac arrest, Sci. Transl. Med. 9 (408) (2017) eaan0117.
[40] E. Brauchle, S. Thude, S.Y. Brucker, K. Schenke-Layland, Cell death stages in single apoptotic and necrotic cells monitored by Raman microspectroscopy, Sci. Rep. 4 (2014) 4698.
[41] I. Notingher, L.L. Hench, Raman microspectroscopy: a noninvasive tool for studies

of individual living cells in vitro, Expet Rev. Med. Dev. 3 (2) (2006) 215–234.
[42] R.J. Holmila, S.A. Vance, X. Chen, H. Wu, K. Shukla, M.S. Bharadwaj, J. Mims, Z. Wary, G. Marrs, R. Singh, A.J. Molina, L.B. Poole, S.B. King, C.M. Furdui, Mitochondria-targeted probes for imaging protein sulfenylation, Sci. Rep. 8 (1) (2018) 6635.
[43] D. Morin, R. Zini, H. Ligeret, W. Neckameyer, S. Labidalle, J.P. Tillement, Dual effect of ebselen on mitochondrial permeability transition, Biochem. Pharmacol. 65 (10) (2003) 1643–1651.
[44] R.L. Puntel, D.H. Roos, R.L. Seeger, J.B. Rocha, Mitochondrial electron transfer chain complexes inhibition by different organochalcogens, Toxicol. Vitro 27 (1) (2013) 59–70.
[45] C.H. Yokomizo, F.S. Pessoto, T. Prieto, R.L. Cunha, I.L. Nantes, Effects of trichlorotelluro-dypnones on mitochondrial bioenergetics and their relationship to the reactivity with protein thiols, Chem. Res. Toxicol. 28 (6) (2015) 1167–1175.
[46] F. Yin, H. Sancheti, E. Cadenas, Mitochondrial thiols in the regulation of cell death pathways, Antioxidants Redox Signal. 17 (12) (2012) 1714–1727.
[47] B.G. Hill, A.N. Higdon, B.P. Dranka, V.M. Darley-Usmar, Regulation of vascular smooth muscle cell bioenergetic function by protein glutathiolation, Biochim. Biophys. Acta 1797 (2) (2010) 285–295.
[48] V. Gupta, K.S. Carroll, Sulfenic acid chemistry, detection and cellular lifetime, Biochim. Biophys. Acta 1840 (2) (2014) 847–875.
[49] J. Talib, M.J. Davies, Exposure of aconitase to smoking-related oxidants results in iron loss and increased iron response protein-1 activity: potential mechanisms for iron accumulation in human arterial cells, J. Biol. Inorg. Chem. 21 (3) (2016) 305–317.
[50] A.P. Halestrap, What is the mitochondrial permeability transition pore? J. Mol. Cell. Cardiol. 46 (6) (2009) 821–831.
[51] D. Morin, S. Barthelemy, R. Zini, S. Labidalle, J.P. Tillement, Curcumin induces the mitochondrial permeability transition pore mediated by membrane protein thiol oxidation, FEBS Lett. 495 (1–2) (2001) 131–136.
[52] A.J. Kowaltowski, R.F. Castilho, A.E. Vercesi, Mitochondrial permeability transition and oxidative stress, FEBS Lett. 495 (1–2) (2001) 12–15.
[53] G.P. McStay, S.J. Clarke, A.P. Halestrap, Role of critical thiol groups on the matrix surface of the adenine nucleotide translocase in the mechanism of the mitochondrial permeability transition pore, Biochem. J. 367 (2) (2002) 541–548.
[54] Y.T. Yang, M. Whiteman, S.P. Gieseg, HOCl causes necrotic cell death in human monocyte derived macrophages through calcium dependent calpain activation, Biochim. Biophys. Acta 1823 (2) (2012) 420–429.
[55] D. Le-Quoc, K. Le-Quoc, Relationships between the NAD(P) redox state, fatty acid oxidation, and inner membrane permeability in rat liver mitochondria, Arch. Biochem. Biophys. 273 (2) (1989) 466–478.
[56] A.P. Halestrap, A pore way to die: the role of mitochondria in reperfusion injury and cardioprotection, Biochem. Soc. Trans. 38 (4) (2010) 841–860.
[57] P.T. Doulias, M. Tenopoulou, J.L. Greene, K. Raju, H. Ischiropoulos, Nitric oxide regulates mitochondrial fatty acid metabolism through reversible protein S-nitrosylation, Sci. Signal. 6 (256) (2013) rs1.
[58] L. Yu, J.X. Xu, P.E. Haley, C.A. Yu, Properties of bovine heart mitochondrial cytochrome b560, J. Biol. Chem. 262 (3) (1987) 1137–1143.
[59] M. Marie, K. Bigot, C. Angebault, C. Barrau, P. Gondouin, D. Pagan, S. Fouquet, T. Villette, J.A. Sahel, G. Lenaers, S. Picaud, Light action spectrum on oxidative stress and mitochondrial damage in A2E-loaded retinal pigment epithelium cells, Cell Death Dis. 9 (3) (2018) 287.
[60] M. Whiteman, P. Rose, J.L. Siau, N.S. Cheung, G.S. Tan, B. Halliwell, J.S. Armstrong, Hypochlorous acid-mediated mitochondrial dysfunction and apoptosis in human hepatoma HepG2 and fetal liver cells: role of mitochondrial permeability transition, Free Radic. Biol. Med. 38 (2005) 1571–1584.